Hindawi Publishing Corporation
Journal of Nanomaterials
Volume 2012, Article ID 853021, 5 pages
doi:10.1155/2012/853021

Research Article

Study of High Quality Indium Nitride Films Grown on Si(100) Substrate by RF-MOMBE with GZO and AlN Buffer Layers

Wei-Chun Chen[1] and Shou-Yi Kuo[2]

[1] *Instrument Technology Research Center, National Applied Research Laboratories, 20 R&D Road VI, Hsinchu Science Park, Hsinchu, 30076, Taiwan*
[2] *Department of Electronic Engineering, Chang Gung University, 259 Wen-Hwa 1st Road, Kwei-Shan, Tao-Yuan 333, Taiwan*

Correspondence should be addressed to Wei-Chun Chen, weichun0809@gmail.com

Received 17 September 2012; Revised 22 November 2012; Accepted 22 November 2012

Academic Editor: Li Li

Wurtzite structure InN films were prepared on Si(100) substrates using radio-frequency metal-organic molecular beam epitaxy (RF-MOMBE) system. Ga-doped ZnO (GZO) and Amorphous AlN (a-AlN) film were used as buffer layers for InN films growth. Structural, surface morphology and optical properties of InN films were investigated by X-ray diffraction (XRD), field emission scanning electron microscopy (FE-SEM), transmission electron microscopy (TEM), and photoluminescence (PL). XRD results indicated that all InN films exhibited preferred growth orientation along the c-axis with different intermediate buffers. TEM images exhibit the InN/GZO growth by two-dimensional mode and thickness about 900 nm. Also, the InN films can be obtained by growth rate about ~1.8 μm/h. Optical properties indicated that the band gap of InN/GZO is about 0.79 eV. These results indicate that the control of buffer layer is essential for engineering the growth of InN on silicon wafer.

1. Introduction

Indium nitride (InN) is a potentially important material for optoelectronic and high speed electronic devices, due to its narrow band gap (<0.7 eV) [1] and superior properties [2], such as high electron mobility [3], small electron effective mass [4], and low carrier concentration [5, 6]. The theoretical maximum mobility calculated for wurtzite (*2H*) InN at 300 K is ~14000 cm^2/V-s [7], while at 77 K the limits are beyond 30000 cm^2/V-s. InN is expected to be used for fabrication of high performance high electron mobility transistors (HEMTS), light-emitting diodes (LEDs) and high efficiency solar cells [8]. The early studies reporting the InN band gap to be ~2 eV were limited by material grown by RF-sputtering [9]. Recent experiments performed on high-quality InN InN films grown by molecular-beam epitaxy MBE have shown unambiguously that the fundamental band gap of InN is about 0.7 eV [10]. The discrepancy in band-gap could be attributed to the crystallinity, carrier concentration, defects, and impurities present in the InN material (such as O, H, C) [11, 12]. Although explanations including the incorporation of oxygen and the Burstein-Moss shift have been proposed, the actual roles of these effects have not been clarified. With the improvement of growth techniques in the past few years, as such as high-quality InN epilayers grown by molecular beam epitaxy (MBE) [13], radio-frequency metal-organic molecular beam epitaxy (RF-MOMBE) [14], sputtering [15], and metal organic chemical vapor deposition (MOCVD) [16] are now readily available. However, the growth of high quality InN films is known to be difficult due to a lack of suitable substrates materials that are matched with InN in terms of both lattice constant and thermal expansion coefficient. Also, the main problems of producing InN thin films are low dissociation temperature of InN [17], and the high equilibrium vapor pressure of nitrogen and lattice mismatch between film and substrate. A variety of templates, namely, GaN and AlN buffer layers on Si and sapphire substrates have been employed for the growth of InN continuous film [18]. However, the lattice mismatch between InN and ZnO, AlN are about 8.9% and 13%, respectively. Compared with InN and sapphire is far below the mismatch of 25.4%. As the result of large lattice mismatch, these

structures contain a very high density of various defects. The effect of growth parameters of InN films such as the substrate temperature, RF power, and In/N flow ratio has been investigated to optimize sample quality [19]. Previous studies of InN deposition on oxide layer show that InN has the highly oriented in the *c*-axis direction [20]. The oxide buffer layer could be a suitable buffer layer for the growth of high-quality InN films. Therefore, low lattice mismatch layer improved the InN nucleation with a high quality [21]. Also, silicon is a very promising material for the growth of III-V materials. With its good thermal conductivity which is especially interesting for electronic applications [22] but also for low-cost high brightness light emitting diodes (LEDs) applications [23]. However, few studies report indicated that InN thin films growth on Si(100) substrate using radio-frequency metal-organic molecular-beam epitaxy (RF-MOMBE).

In this work, we studied the effect of different buffer layers on the growth of InN by radio-frequency metal-organic molecular-beam epitaxy (RF-MOMBE). As a result of these investigations, we found that the high quality InN layers on a Si(100) substrate is obtained using the GZO buffer layer. Characterization of crystallinity, surface morphology, and emission property was investigated by X-ray diffraction (XRD), scanning electron microscopy (SEM), transmission electron microscopy (TEM), and photoluminescence (PL) measurement. Also, the influence of growth parameters on the InN samples was discussed in detail.

2. Experiment

InN films were grown by radio-frequency metal-organic molecular beam epitaxy (RF-MOMBE) with Ga-doped ZnO (GZO) layer, amorphous AlN (a-AlN) layer, and direct growth on Si(100) substrate. The growth chamber of RF-MOMBE system was vacuumed to a base pressure of 10^{-7} Pa by a turbo molecular pump. Trimethylaluminum (TMA), trimethylindium (TMI) were used as the group-III precursors without any carrier gas. The temperatures of precursors were kept at 65°C for TMI and 20°C for TMAl. Atomic nitrogen generated by radio-frequency (RF) plasma was used as the group-V source. The 240 nm-GZO film was deposited on Si(100) using RF-sputtering at 300°C with working pressure $\sim 10^{-1}$ Pa. Before loading substrate into the chamber, the Si(100) substrates were cleaned in an ultrasonic bath with acetone and ethanol, and the Si(100) substrates were also etched in a 5% HF solution for 3 min to remove the oxide on the surface.

Before the a-AlN growth, silicon substrate was thermally cleaned at 900°C for 30 min in vacuum chamber with 10^{-7} Pa. Then, the substrate temperature was decreased to 850°C at 5 min for nitridation, followed by the growth of a-AlN layer at 750°C. Finally, the InN films were deposited on GZO, a-AlN buffer layers and Si(100) substrate at 500°C for 30 min. During the deposition, the substrate temperature was monitored by a thermocouple.

X-ray diffraction (XRD) including θ-2θ scan was carried out on a Bede D1 X-ray diffractometer with a CuKα radiation source. The surface morphologies and cross-section of InN films were obtained by field-emission scanning electron microscopy (FE-SEM) (Hitachi S4300). The microstructures of the InN films were investigated in detail by transmission electron microscopy (TEM) in cross-sectional configuration (TEM, Philips Tecnai 20). The optical property was performed by photoluminescence (PL) measurements. A diode laser operating at a wavelength of 976 nm was used as the excitation source.

3. Results

Figure 1(a) shows that the XRD pattern of high preferred orientation GZO thin film grown on Si(100) substrate by RF-sputtering which narrow full-width half maximum (FWHM) of (0002) diffraction peak is about 400 arcsec. Also, selected-area diffraction pattern (SAD) observed the nearly-single crystal structure. Figure 1(b) shows the θ-2θ XRD pattern of the InN films growth on GZO, a-AlN, and direct deposition on Si(100) substrate, respectively. The observed diffraction peak exhibited dominant InN (0002) peak at ~31.3° for all samples, revealing that the InN films mainly consisted of the hexagonal InN phase. Diffraction peaks corresponding to the (0002) and (0004) from InN film, (0002) form GZO film, and the (400) diffraction peak from Si(100) are observed for InN/GZO sample. Compared with direct deposition on Si(100) substrate, the InN/GZO exhibited highly *c*-axis preferred orientation indicating that it have relative narrow peak with good crystalline quality. In addition, InN grown on a-AlN and Si(100) exhibited polycrystalline structure and random growth. Also, a smaller peak corresponding to the indium metal detected in the XRD pattern for InN/AlN and InN/Si(100) samples, which is probably due to the slightly In-rich conditions. Also, three prominent XRD peaks, corresponding to InN (100), (0002), (101), and In(101) were observed for InN film grown directly on the Si(100) substrate, while there is no indium oxide peak in the XRD spectra. According to these results, the GZO buffer layer can be provided InN nucleation and improvement quality due to smaller lattice mismatch (~8.9 %). From the observed (0002) diffraction the lattice parameter *c* can be obtained. InN/GZO shows the large than the value of the bulk crystal [24] attributed to the residual strain in the InN film.

Figure 2 shows the 30° Plan-view and cross-sectional SEM images of InN films grown on various buffer layers. Cross-section image of InN/GZO film indicated that thickness of GZO film is about 240 nm. The image reveals that the InN/GZO film exhibits a pronounced columnar-structure at 500°C. Also, surface morphology of InN film shows the needle-like nanocrystals. In addition, an InN/a-AlN film reveals the granular structure of surface morphology. Also, surface roughness is larger than InN growth on GZO layer due to high density grain boundaries and island growth. The InN film directly grown on Si(100) exhibits surface morphology of noncontinuous and rough features. The result is due to a stress induced 3D-growth mechanism caused by a lattice strain and/or higher desorption rate (>1.5 μm/hr). Also, the formation of metallic In on the surface was observed which corresponding to XRD result.

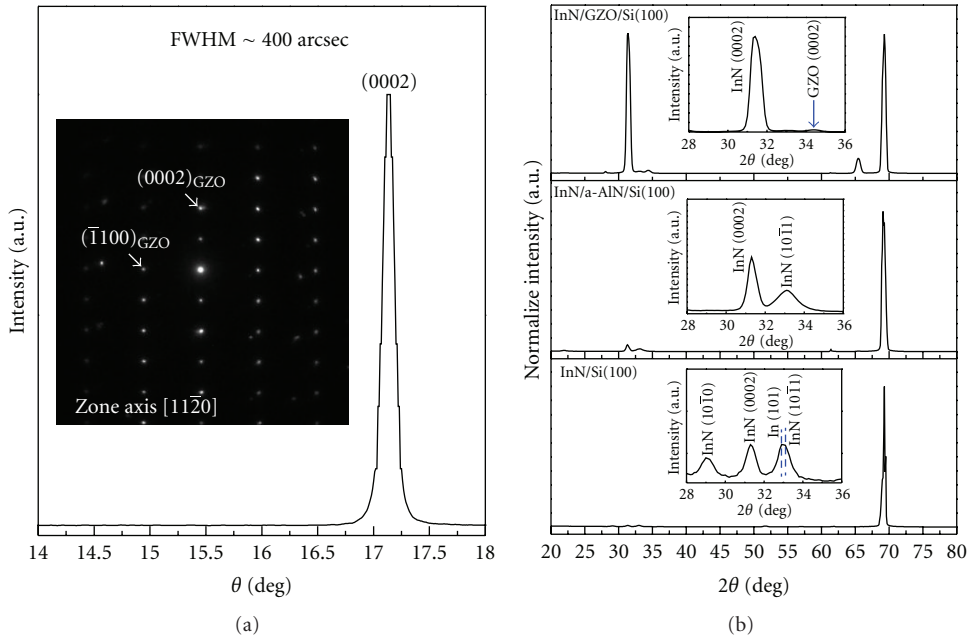

Figure 1: (a) XRD pattern of a sputtered GZO film and (b) θ-2θ XRD patterns of InN film deposited on various buffer layers.

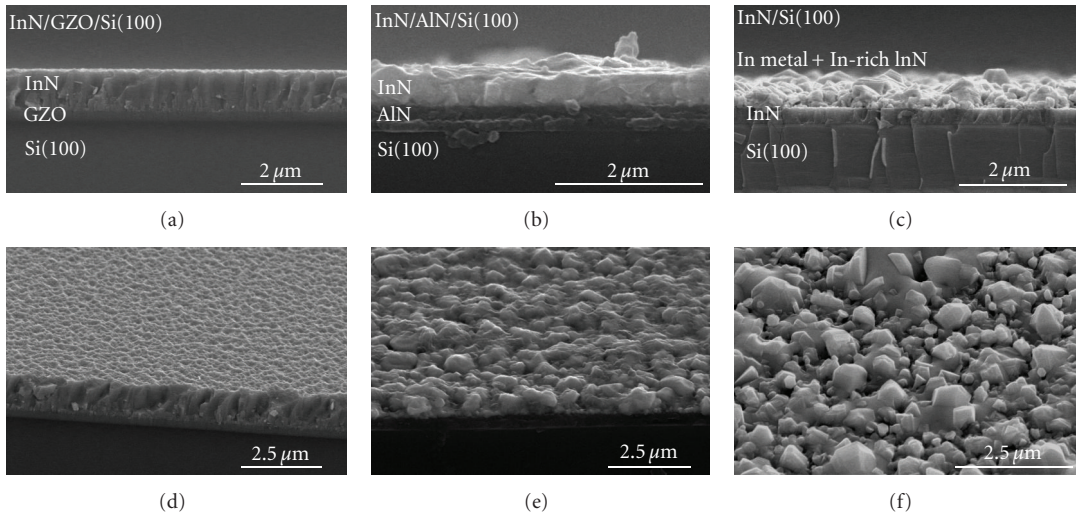

Figure 2: SEM cross-sectional and surface morphologies images of InN film were grown on various buffer layers.

Figure 3 shows a cross-sectional bright-field TEM images for the InN films growth on GZO and a-AlN buffer layers. Figure 3(a) shows that 900 nm-thick InN film grown on GZO buffer layer clearly observed that the threading dislocations (TDs) and stacking faults are near the interface. Also, no obvious indium metal precipitates are seen in image. Besides, cross-sectional bright-field TEM image of InN/GZO film observed along the [10$\bar{1}$0] direction. The lattice fringes reveal that the *c*-axis lattice parameter of the InN/GZO is about 0.588 nm, which is larger than bulk InN [25], suggesting that the lattice strain of InN is not significantly relaxed after the growth may be due to oxygen content in the films, toward the formation of In_2O_3 [26]. Figure 3(b) shows InN film grown on Si(100) with a-AlN buffer layer. The *c*-axis lattice parameter of InN/AlN film was measured to be about 0.57 nm which is matched to the value of bulk InN, suggesting that the InN is near fully-relaxed at after growth. This result is in good agreement with the theoretical calculated values from XRD measurement. Also, selected-area electron diffraction pattern (SAED) of all InN films reveals a hexagonal wurtzite structure with an incident beam direction of <0001> is clearly observed. No additional diffraction spots were observed in the pattern. On the other hand, the SAED of InN/AlN shows a typical characteristic of a nearly-single crystalline. Also, it can be seen clearly that the film was 3D growth mode.

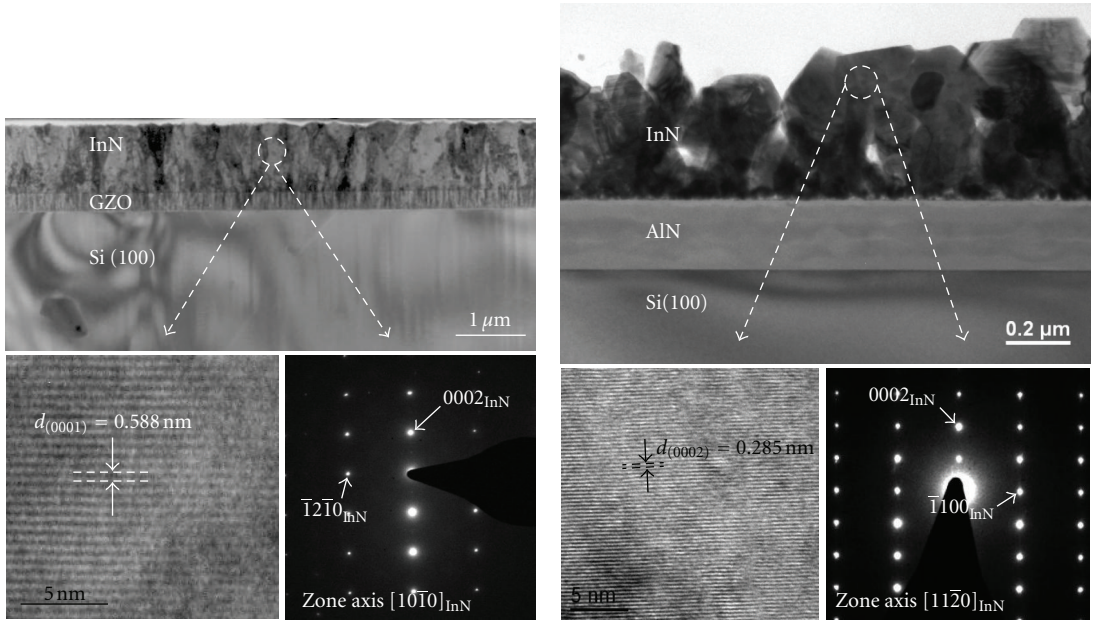

Figure 3: Cross-sectional TEM image of typical InN area with the corresponding SAED pattern shows from (a) InN/GZO film and (b) InN/a-AlN film.

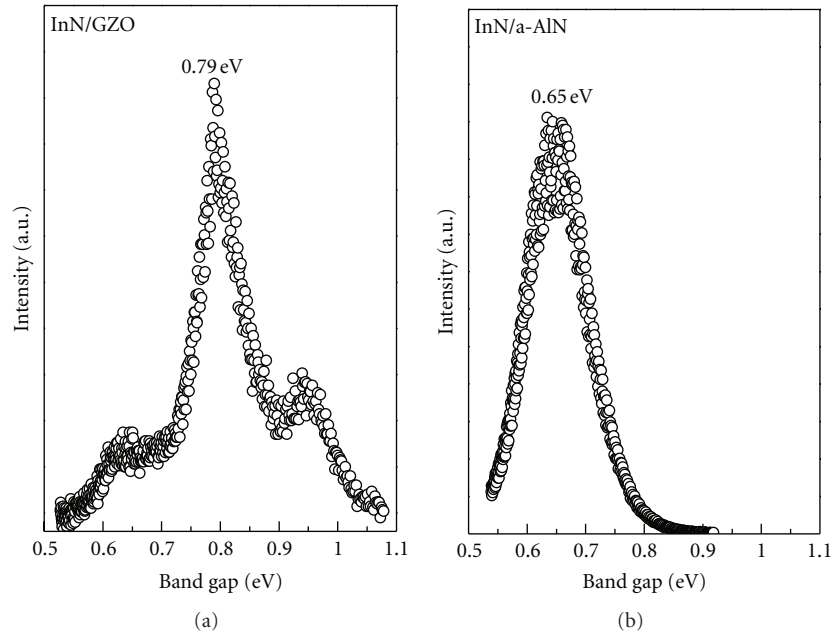

Figure 4: Room temperature PL spectra of InN films grown on Si(100) with different buffer layers.

Figure 4 shows the PL spectra measurement at room temperature from an InN film deposited on GZO and AlN layer at 500°C. The PL result indicated sample fundamental band gap was located at InN/GZO about 0.79 eV and InN/AlN about 0.65 eV. In contrast with our previous studies [27], InN grown on oxide layer exhibited large band gap due to high carrier density and oxygen incorporation [28]. Also, the origin of the higher measured band gaps in these films can be attributed to the presence of In_2O_3 (Eg = 3.75 eV) [29] inclusions and, perhaps, to a blue-shift of the absorption edge from quantum-size effects caused by the needle-like [30]. In addition, the intrinsic defects such as N vacancies and/or dislocations could be important additional sources for free electrons in these samples. The Hall measurements of the InN/GZO exhibited a high carrier concentration of 2.6×10^{20} cm^{-3} and electron mobility of 78 cm^2/V-s. Therefore,

we infer that fewer defects and the low background carrier concentration were cause of influence high quality InN.

4. Conclusion

In summary, the high quality InN grown on Si(100) substrate with the GZO buffer layer is critical to achieve nucleation and duplicate orientation. The XRD measurement indicates that the InN films are highly oriented in the *c*-axis direction. According to XRD and TEM results, the GZO buffer layer improved the crystal quality effectively which was smaller surface roughness. The PL results reveal that band gap was located at InN/GZO about 0.79 eV. Also, the high background-carrier concentration may be caused by a structural defect and/or oxygen incorporation.

References

[1] C. L. Hsiao, H. C. Hsu, L. C. Chen et al., "Photoluminescence spectroscopy of nearly defect-free InN microcrystals exhibiting nondegenerate semiconductor behaviors," *Applied Physics Letters*, vol. 91, Article ID 181912, 3 pages, 2007.

[2] A. G. Bhuiyan, A. Hashimoto, and A. Yamamoto, "Indium nitride (InN): a review on growth, characterization, and properties," *Journal of Applied Physics*, vol. 94, no. 5, pp. 2779–2808, 2003.

[3] C. A. Chang, C. F. Shih, N. C. Chen, T. Y. Lin, and K. S. Liu, "In-rich $In_{1-x}Ga_xN$ films by metalorganic vapor phase epitaxy," *Applied Physics Letters*, vol. 85, no. 25, pp. 6131–6133, 2004.

[4] S. P. Fu and Y. F. Chen, "Effective mass of InN epilayers," *Applied Physics Letters*, vol. 85, no. 9, pp. 1523–1525, 2004.

[5] T. Inushima, M. Haigashiwaki, T. Matsui, T. Takenobu, and M. Motokawa, "Electron density dependence of the electronic structure of InN epitaxial layers grown on sapphire (0001)," *Physical Review B*, vol. 72, no. 8, Article ID 085210, 10 pages, 2005.

[6] B. E. Foutz, S. K. O'Leary, M. S. Shur, and L. F. Eastman, "Transient electron transport in wurtzite GaN, InN, and AlN," *Journal of Applied Physics*, vol. 85, no. 11, pp. 7727–7734, 1999.

[7] V. M. Polyakov and F. Schwierz, "Low-field electron mobility in wurtzite InN," *Applied Physics Letters*, vol. 88, Article ID 032101, 3 pages, 2006.

[8] V. Ya. Malakhov, "Potential PV materials-based InN thin films: fabrication, structural and optical properties," *Solar Energy Materials and Solar Cells*, vol. 76, no. 4, pp. 637–646, 2003.

[9] H. J. Hovel and J. J. Cuomo, "Electrical and optical properties of rf-sputtered GaN and InN," *Applied Physics Letters*, vol. 20, no. 2, pp. 71–73, 1972.

[10] J. Wu, W. Walukiewicz, K. M. Yu et al., "Unusual properties of the fundamental band gap of InN," *Applied Physics Letters*, vol. 80, no. 21, pp. 3967–3969, 2002.

[11] J. Wu, W. Walukiewicz, S. X. Li et al., "Effects of electron concentration on the optical absorption edge of InN," *Applied Physics Letters*, vol. 84, no. 15, pp. 2805–2807, 2004.

[12] K. Sugita, A. Hashimoto, and A. Yamamoto, "Effect of oxygen supply on MOVPE InN," *Physica Status Solidi (C)*, vol. 6, no. 2, pp. S389–S392, 2009.

[13] J. Kamimura, T. Kouno, S. Ishizawa, A. Kikuchi, and K. Kishino, "Growth of high-In-content InAlN nanocolumns on Si (1 1 1) by RF-plasma-assisted molecular-beam epitaxy," *Journal of Crystal Growth*, vol. 300, no. 1, pp. 160–163, 2007.

[14] H. Naoi, F. Matsuda, T. Araki, A. Suzuki, and Y. Nanishi, "The effect of substrate polarity on the growth of InN by RF-MBE," *Journal of Crystal Growth*, vol. 269, no. 1, pp. 155–161, 2004.

[15] T. Sasaoka, M. Mori, T. Miyazaki, and S. Adachi, "Room-temperature infrared photoluminescence from sputter-deposited InN films," *Journal of Applied Physics*, vol. 108, no. 6, Article ID 063538, 5 pages, 2010.

[16] P. Singh, P. Ruterana, M. Morales et al., "Structural and optical characterisation of InN layers grown by MOCVD," *Superlattices and Microstructures*, vol. 36, no. 4–6, pp. 537–545, 2004.

[17] J. B. MacChesney, P. M. Bridenbaugh, and P. B. O'Connor, "Thermal stability of indium nitride at elevated temperatures and nitrogen pressures," *Materials Research Bulletin*, vol. 5, no. 9, pp. 783–791, 1970.

[18] H. Lu, W. J. Schaff, J. Hwang, H. Wu, G. Koley, and L. F. Eastman, "Effect of an AlN buffer layer on the epitaxial growth of InN by molecular-beam epitaxy," *Applied Physics Letters*, vol. 79, no. 10, pp. 1489–1491, 2001.

[19] J. Grandal and M. A. Sánchez-García, "InN layers grown on silicon substrates: effect of substrate temperature and buffer layers," *Journal of Crystal Growth*, vol. 278, no. 1–4, pp. 373–377, 2005.

[20] F. I. Lai, S. Y. Kuo, W. T. Lin et al., "Photoluminescence studies of indium nitride films grown on oxide buffer by metalorganic molecular-beam epitaxy," *Journal of Crystal Growth*, vol. 320, no. 1, pp. 32–35, 2011.

[21] T. Ohgaki, N. Ohashi, H. Haneda, and A. Yasumori, "Molecular beam epitaxy growth of indium nitride films on c-face zinc oxide substrates," *Journal of Crystal Growth*, vol. 292, no. 1, pp. 33–39, 2006.

[22] J. D. Brown, R. Borges, E. Piner, A. Vescan, S. Singhal, and R. Therrien, "AlGaN/GaN HFETs fabricated on 100-mm GaN on silicon (111) substrates," *Solid-State Electronics*, vol. 46, no. 10, pp. 1535–1539, 2002.

[23] A. Dadgar, C. Hums, A. Diez, F. Schulze, J. Blasing, and A. Krost, "Epitaxy of GaN LEDs on large substrates: Si or sapphire?" in *Advanced LEDs for Solid State Lighting*, vol. 6355, 63550R of *Proceedings of SPIE*, 2006.

[24] W. Paszkowicz, R. Černý, and S. Krukowski, "Rietveld refinement for indium nitride in the 105–295 K range," *Powder Diffraction*, vol. 18, pp. 114–121, 2003.

[25] T. L. Tansley and C. P. Foley, "Optical band gap of indium nitride," *Journal of Applied Physics*, vol. 59, no. 9, pp. 3241–3244, 1986.

[26] A. G. Bhuiyan, K. Sugita, K. Kasashima, A. Hashimoto, A. Yamamoto, and V. Yu. Davydov, "Single-crystalline InN films with an absorption edge between 0.7 and 2 eV grown using different techniques and evidence of the actual band gap energy," *Applied Physics Letters*, vol. 83, no. 23, p. 4788, 2003.

[27] S. Y. Kuo, F. I. Lai, W. C. Chen et al., "Epitaxial growth of InN film on intermediate oxide buffer layer by RF-MOMBE," *Diamond and Related Materials*, vol. 20, no. 8, pp. 1188–1192, 2011.

[28] M. Yoshimoto, H. Yamamoto, W. Huang et al., "Widening of optical bandgap of polycrystalline InN with a few percent incorporation of oxygen," *Applied Physics Letters*, vol. 83, no. 17, pp. 3480–3482, 2003.

[29] R. L. Weiher and R. P. Ley, "Optical properties of indium oxide," *Journal of Applied Physics*, vol. 37, no. 1, pp. 299–302, 1966.

[30] V. Yu. Davydov, A. A. Klochikhin, V. V. Emtsev, F. Bechstedt, A. V. Mudryi, and E. E. Haller, "Reply to "comment on "band gap of InN and In-Rich $In_xGa_{1-x}N$ alloys ($0.36 < x < 1$)"","" *Physica Status Solidi (B)*, vol. 233, no. 3, pp. R10–R11, 2002.